Running title: Identifying interaction partners of reticulons

Author for correspondence:

Dr Verena Kriechbaumer

Plant Cell Biology

Biological and Medical Sciences

Oxford Brookes University

Gipsy Lane, Headington

Oxford OX3 0BP, UK

Reticulomics: Protein-protein interaction studies with two plasmodesmata-localised reticulon family proteins identify binding partners enriched at plasmodesmata, ER and the plasma membrane

Verena Kriechbaumer[1], Stanley W. Botchway[2], Susan E Slade[3], Kirsten Knox[4], Lorenzo Frigerio[5], Karl Oparka[4], Chris Hawes[1]

[1] Plant Cell Biology, Biological and Medical Sciences, Oxford Brookes University, Oxford OX3 0BP, UK

[2] Central Laser Facility, STFC Rutherford Appleton Laboratory, RCaH, Didcot OX11 0QX, UK

[3] WPH Proteomics Facility RTP, School of Life Sciences, University of Warwick, Coventry CV4 7AL, UK

[4] Institute of Molecular Plant Sciences, University of Edinburgh, Edinburgh EH9 3JR, UK

[5] School of Life Sciences, University of Warwick, Coventry CV4 7AL, UK

Summary: Protein interactions for two plasmodesmata-localised reticulon proteins suggest that these proteins, in addition to a role in ER modelling, may play important roles in linking ER and plasma membrane.

Funding information: This work was supported by grant BB/J004987/1 from the British Biotechnology and Biological Sciences Research Council (BBSRC) to K.O. and C.H. and the STFC programme access grant Ref No 14230008 to C.H.

Author for correspondence: vkriechbaumer@brookes.ac.uk

Abstract

The ER is a ubiquitous organelle that plays roles in secretory protein production, folding, quality control, and lipid biosynthesis. The cortical ER in plants is pleomorphic and structured as a tubular network capable of morphing into flat cisternae, mainly at three way junctions, and back to tubules. Plant reticulon (RTNLB) proteins tubulate the ER by dimer- and oligomerization, creating localised ER membrane tensions that result in membrane curvature. Some RTNLB ER-shaping proteins are present in the plasmodesmal (PD) proteome (Fernandez-Calvino et al., 2011) and may contribute to the formation of the desmotubule, the axial ER-derived structure that traverses primary PD (Knox et al., 2015). Here we investigate the binding partners of two PD-resident reticulon proteins, RTNLB3 and RTNLB6, that are located in primary PD at cytokinesis (Knox et al., 2015). Co-immunoprecipitation of GFP-tagged RTNLB3 and RTNLB6 followed by mass spectrometry detected a high percentage of known PD-localised proteins as well as plasma-membrane proteins with putative membrane anchoring roles. FRET-FLIM assays revealed a highly significant interaction of the detected PD proteins with the bait RTNLB proteins. Our data suggest that RTNLB proteins, in addition to a role in ER modelling, may play important roles in linking the cortical ER to the plasma membrane.

Introduction

The endoplasmic reticulum (ER) is a multifunctional organelle (Hawes et al., 2015) and is the site of secretory protein production, folding and quality control (Brandizzi et al., 2003) and lipid biosynthesis (Wallis and Browse, 2010), but is also involved in many other aspects of day-to-day plant life including auxin regulation (Friml and Jones, 2010) and oil and protein body formation (Huang, 1996; Herman, 2008). The cortical ER network displays a remarkable polygonal arrangement of motile tubules that are capable of morphing into small cisternae, mainly at the three way junctions of the ER network (Sparkes et al., 2009). The cortical ER network of plants has been shown to play multiple roles in protein trafficking (Palade, 1975; Vitale and Denecke, 1999) and pathogen responses (reviewed in Pattison and Amtmann, 2009; Beck et al., 2012).

In plants, the protein family of reticulons (RTNLBs) contributes significantly to tubulation of the ER (Tolley et al., 2008, 2010; Chen et al., 2012). RTNLBs are integral ER membrane proteins that feature a C-terminal reticulon homology domain (RHD) that contains two major hydrophobic regions. These regions form two “V”-shaped transmembrane wedges joined together via a cytosolic loop, with the C- and N-terminus of the protein facing the cytosol. RTNLBs can dimerize or oligomerize creating localised tensions in the ER membrane, inducing varying degrees of membrane curvature (Sparkes et al., 2010). Hence, RTNLBs are considered to be essential in maintaining the tubular ER network.

The ability of RTNLBs to constrict membranes is of interest in the context of cell-plate development and the formation of primary PD (Knox et al., 2015). PD formation involves extensive remodelling of the cortical ER into tightly furled tubules to form the desmotubules, axial structures that run through the PD pore (Ehlers and Kollmann, 2001; Overall and Blackman, 1996). At only 15 nm in diameter, the desmotubule is one of the most constricted membrane structures found in nature, with no animal counterparts (Tilsner et al., 2011). PD are membrane-rich structures characterized by a close association of the plasma membrane with the ER. The forces that model the ER into desmotubules, however, are poorly understood. RTNLBs are excellent candidates for this process and can constrict fluorescent protein labelled ER membranes into extremely fine tubules (Sparkes et al., 2010). We have shown recently that two of the RTNLBs present in the PD proteome, RTNLB3 and RTNLB6 (Fernadez-Calvino, 2011), are present in primary PD at cytokinesis (Knox et al., 2015). However, nothing is known of the proteins that interact with RTNLBs identified in the PD proteome, or that may link RTNLBs to the plasma membrane (PM). To date, the only protein

shown to bind to plant RTNLBs is RHD3-like2, the plant homologue of the ER tubule fusion protein, atlastin (Lee et al., 2013).

Here we used a dual approach to identify interacting partners of RTNLB3 and RTNLB6 (Fernandez-Calvino et al., 2011; Knox et al*.,* 2015). First, we used GFP-immunoprecipitation assays coupled to mass spectrometry to identify proteins potentially binding to RTNLB3 and RTNLB6. Second, from the proteins we identified, we conducted a detailed FRET-FLIM (Förster Resonance Energy Transfer by Fluorescence Life Time Imaging) analysis to confirm prey-bait interactions *in vivo*.

The application of time resolved fluorescence spectroscopy to imaging biological systems has allowed design and the implementation of Fluorescence Lifetime Imaging Microscopy (FLIM). The technique allows measuring and determining the space map of picosecond fluorescence decay at each pixel of the image through confocal single and multiphoton excitation. The general fluorescence or Förster resonance energy transfer (FRET) to determine co-localisation of two colour chromophores can now be improved to determine physical interactions using FRET-FLIM using protein pairs tagged with appropriate GFP-fluorophores and monomeric red fluorescent protein. FRET-FLIM measures the reduction in the excited state life time of GFP (donor) fluorescence (in the presence of an acceptor fluorophore (e.g. mRFP) which is independent of the problems associated with steady state intensity measurements. the observation of such a reduction is an indication that the two proteins are within a distance of 1 to 10 nm thus indicating a direct physical interaction between the two protein fusions (Osterrieder et al., 2009, Sparkes et al., 2010, Schoberer and Botchway, 2014). It was previously shown that a reduction of as little as ~200 ps in the excited state lifetime of the GFP labelled protein represents quenching through a protein-protein interaction (Stubbs et al., 2005).

Our interaction data identified a large percentage (40%) of ER proteins, including other RTNLB family members. However, we also found a relatively large number (25%) of proteins present in the published PD proteome (Fernadez-Calvino et al., 2011), and a surprisingly high proportion (35%) of plasma membrane proteins. Of the PD-resident proteins we identified, a significant number were shown previously to be targets of viral movement proteins (MPs) or proteins present within lipid rafts, consistent with the view that PD are lipid-rich microdomains (Bayer et al., 2014). Additional proteins identified suggested roles for RTNLBs in transport and pathogen defence. We suggest that RTNLBs may play key roles in anchoring and/or signalling between the cortical ER and PM.

Results

Identification of proteins that interact with RTNLB3 and RTNLB6

The reticulon proteins RTNLB3 and RTNLB6 are found in the PD proteome (Fernandez-Calvino et al., 2011). We have shown recently that when both RTNLBs are co-expressed transiently in tobacco epidermal leaf cells with the viral movement protein (MP) of tobacco mosaic virus (TMV) there is significant co-localisation (Knox et al., 2015). Both these RTNLBs are located to the developing cell plate at cytokinesis, and are therefore strong candidates for proteins that model the cortical ER into desmotubules (Knox et al., 2015).

As it is likely that RTNLBs form protein complexes with proteins in the plasma membrane and desmotubule in order to stabilise the desmotubule constriction and to allow gating in PD (see model in Knox et al., 2015) we searched for potential interacting proteins capable of carrying out these tasks.

To find interaction partners for these RTNLBs, we used Arabidopsis plants stably expressing RTNLB3-YFP or RTNLB6-YFP fusion proteins under a 35S promoter to perform co-immunoprecipitations using GFP-Trap®_A beads (Chromotek). For this approach whole seedling protein extracts were incubated with agarose slurry linked to anti-GFP camelid antibodies. This antibody is capable of binding the YFP-tag on the reticulon proteins. The RTNLB bait, along with the proteins that bind/interact with the RTNLB, were pelleted by slow centrifugation. The resulting proteins in this pellet were identified using mass spectrometry (nanoLC-ESI-MS/MS, Thermo Orbitrap Fusion, Thermo Scientific) and the data analysed using Scaffold Proteome Software (version Scaffold_4.4.1.1, Proteome Software Inc., Portland, OR). As a control, proteins bound to the antibody in untransformed plants were also analysed by MS.

The MS data showed a high percentage of overlay between proteins identified with RTNLB3 and RTNLB6 as baits (Figure 1). Of a total of 706 identified proteins only 93 (13%) or 85 (12%) proteins were unique to RTNLB3 or RTNLB6, respectively (Table 1). Proteins that were also identified in the control samples (two independent sets of wildtype Arabidopsis plants) were subtracted from the list of proteins resulting in 146 potential interacting partners for either RTNLB3 or RTNLB6. Despite the removal of false positives, a high percentage of proteins in common was maintained for both reticulons: out of a total of 146 proteins, RTNLB3 had 135 potential interaction candidates with only with only 11 proteins (8%) showing unique specificity

for RTNLB3. Similarly, 126 proteins were co-immunoprecipitated with RTNLB6, with 20 proteins (17%) being unique to RTNLB6 (Table 1).

These resulting protein candidates were ranked according to their 'percentage of the total spectra', which represents the number of spectra matching a specific protein (across all MS samples) as a percentage of the total number of spectra in the sample (Supplemental Table 1). This ranking indicates the amount of a specific protein bound to the RTLNB-baits and can therefore be used as a measure of the reliability of each potential interaction.

FRET-FLIM analysis to validate immunoprecipitation data

17 proteins from the list of 146 potential interacting proteins were subjected to further analysis to test for interactions *in vivo* using a different methodology (FRET-FLIM; Table 1, Table 2). The choice of these 17 proteins was based on three main criteria:

i) Known or expected interacting partners of RTNLBs from published work. These were used as positive controls and included; RTNLB3 and RTNLB6 (RTNLB3 dimerization in Sparkes et al., 2010) and RHD3/RL2 (Lee et al., 2013);

ii) Proteins present in the PD proteome, listed in Table 2.

iii) A selection of low-abundance proteins distributed throughout the quantitative lists (see Table 2, Supplemental Table 1). These were used to test the hypothesis that proteins with low abundance in the GFP-Trap assays were likely to represent weak or false-positive interactions. For example, thioredoxin 3 (TRX3; Table 2) showed very low abundance relative to, for example, DWARF1 (DWF1).

iv) TCP-1/cpn60 chaperonin family protein (TCP1) was chosen as a further control as this protein was found in the proteome for RTNLB3 but not for RTNLB6 (Table 2, Supplemental Table 1).

Förster resonance energy transfer (FRET; Förster, 1948) measured by donor-excited state fluorescence lifetime imaging (FLIM; Becker, 2012; Schoberer and Botchway, 2014) was used to confirm independently the interactions suggested by the GFP-Trap assays. FRET-FLIM measures the reduction in the lifetime of the GFP (donor) fluorescence when an acceptor fluorophore (mRFP) is within a distance of 1 to 10 nm, thus allowing FRET to occur and indicating a physical interaction between the two protein fusions (Osterrieder et al., 2009, Sparkes et al., 2010). In the FRET-FLIM assay, each of the above 17 proteins was expressed transiently as an mRFP fusion (acceptor) in tobacco leaf epidermal cells expressing either RTNLB3-GFP or RTNLB6-GFP as donors. At least two biological samples with a minimum of three technical replicates each were used for the statistical analysis.

Due to limitations in the speed of photon counting of the FLIM apparatus, measurements were taken from high expressing areas of ER regions with relatively low mobility, such as the ER associated with the nuclear envelope. This allowed more reliable measurements than the fast moving cortical ER (see Sparkes et al., 2010). Furthermore, to allow consistent and reliable measurements also proteins that usually localise to PD or PM were driven to the ER by protein overexpression. FRET-FLIM interactions are shown in Table 2. RTNLB3-GFP or RTNLB6-GFP expression without acceptor presence was used as a negative control while known self-interactions between the RTNLBs (e.g. RTNLB3 against RTNLB3) or with the second RTNLB (e.g. RTNLB3 against RTNLB6) were used as positive controls and to determine the value of fluorescence that could be considered as a significantly positive interaction. Figure 2 shows a comparison of such negative and positive controls:

RTNLB3-GFP alone showed a fluorescence lifetime of 2.47±0.05 ns, and RTNLB6-GFP alone a lifetime of 2.63±0.06 ns. Excited state lifetimes determined for RTNLB-RTNLB homomeric and heteromeric interactions varied from 2.31 to 2.38 ns (Table 3) which is statistically significantly different to that of the GFP alone. Figure 2 shows the FRET-FLIM analysis steps for RTNLB6-GFP alone (Figure 2 A-D) as a negative control, and for RTNLB6-GFP interacting with RFP-RTNLB6 (Figure 2 E-I) as a positive control. Raw FRET-FLIM images are shown in Figure 2 A and E. This analysis takes into account the lifetime values of each pixel within the image visualised by a pseudo-coloured lifetime map (Figure 2 B and F). The graph shows the distribution of lifetimes within the image (Figure 2 C and G) with blue shades representing longer GFP fluorescence lifetimes than green ones. Decay curves (Figure 2 D and H) of a representative single pixel highlight an optimal single exponential fit, where Chi square (χ^2) values from 0.9 to 1.2 were considered an excellent fit to the data points (binning factor of 2). Confocal pictures for the region of interest showing the GFP-construct in green and the mRFP-construct in red are shown in Figure 2 A (inset) and I. This specific example shows that RTNLB6 homodimerizes because the lifetime values for the GFP/mRFP fusion pair (2.38±0.01 ns, Table 3) are lower than those for the GFP fusion alone (2.63±0.06 ns).

Next, RTNLB3-GFP and RTNLB6-GFP were co-infiltrated independently with each of the 17 chosen proteins and the resulting lifetimes measured (Table 3, Figure 3). Representative FRET-FLIM data are shown for each combination (Supplemental Figure S1). As mentioned above, ER regions with relatively low mobility, such as the ER associated with the nuclear envelope allow more reliable measurements (Sparkes et al., 2010). Therefore, to be comparable with other data the interactions between RTNLBs and PM -localised proteins such as remorins and PIP3 were also measured in this area. These PM–bound proteins are also normally detected as they transit through the ER in transient expression experiments.

Among the RTNLB3 putative interactors, all proteins with the exceptions of FASCICLIN-like arabinogalactan protein 8 (FLA8), annexin 4 (ANNAT4) and thioredoxin 3 (TRX3) showed interaction. Significantly, these proteins were not present in the second MS dataset (Table 2), and their lack of interaction using FRET-FLIM confirmed that these were likely to be false positives. The results for TCP1 are also significant because TCP1 was pulled down by RTNLB3, but not by RTNLB6, and in the FRET-FLIM assays TCP1 interacted with RTNLB3 but not with RTNLB6, confirming the results of the GFP-Trap data. (Table 3, Figure 3). To summarise, the proteomics data from one biological sample yielded less than 18% false-negatives in the chosen selection with the three false-negative proteins showing comparatively low peptide coverage.

Mass spectrometry confirmation of proteomics data

For further confirmation of the data, the GFP-Immunoprecipitation and MS proteomics was repeated with an independent biological sample of RTNLB3-YFP and RTNLB6-YFP plants, as well as wild-type Arabidopsis and a stable Arabidopsis line expressing the ER-membrane marker calnexin (CXN) tagged with GFP. The ER-integral protein calnexin was used to detect false-positive interactions resulting from proteins binding to the fluorescent tag rather than the RTNLBs. Results from the wildtype and CXN immunoprecipitations were subtracted from the proteins pulled down with RTNLB3 or RTNLB6. This second dataset was then compared with data from the first experiment and only proteins present in both datasets compiled into a final list of interaction candidates (Table 4, Supplemental Table 2).

This resulted in 42 interaction candidates for RTNLB3 and 57 for RTNLB6. Proteins were again ranked according to the quantity of peptide present in the total spectra. Interestingly proteins that were identified by FRET-FLIM to be false-positives in the first MS run (FLA8, ANNAT4 and TRX3) were not present in the second MS dataset thereby confirming and validating the FRET-FLIM methodology (Table 2). The final list of interaction candidates comprises furthermore a high percentage of proteins localised or predicted to be localised to PD and ER (Figure 4).

Discussion

Validation of the proteomics approach

Immunoprecipitation using the camelid GFP-Trap system with two of the PD proteome reticulons, RTNLB3 and RTNLB6 (Fernandez-Calvino et al., 2011; Knox et al., 2015), identified a high percentage of PD-localised proteins and also proteins that are more widely

distributed over the ER and PM. These proteomics data were validated by *in vivo* testing with FRET-FLIM, and further rounds of immunoprecipitation using different controls confirmed the initial data and removed the few proteins that did not interact *in vivo,* indicating that these were most likely false positives. The following points are stressed:

a) FRET-FLIM analysis corresponded with the second mass spec run: In the FRET-FLIM analysis for both RTNLB3 and RTNLB6 FLA8, ANNAT4 and TRX3 did not show a decreased florescence lifetime (Table 3, Figure 3). There proteins were absent from the second MS data set for both reticulons and were therefore most likely false-positives in the first MS run. Additionally FLA8, ANNAT4 and TRX3 showed low peptide abundances in the MS spectra (Table 2) indicating a higher rate of false positives in the lower ranges of abundance.

b) TCP1 was pulled down with RTNLB3 but not with RTNLB6 (Table 3, Figure 3) and indeed FRET-FLIM analysis showed interaction of TCP1 with RTNLB3 but not RTNLB6 validating both the proteomics data and the FRET-FLIM approach as a confirmatory method.

c) Selectivity of reticulon protein-protein interactions: Out of 21 Arabidopsis reticulons, some of which have been shown to interact previously (Sparkes et al., 2010), only RTNLB3, RTNLB6, RTNLB5 and RTNLB1 showed up as interactors in the immunoprecipitation analysis with the bait PD reticulons RTNLB3 and RTNLB6 (Table 4, Supplemental Table 2). RTNLB5 is 84% identical at the amino acid level with RTNLB6 and therefore difficult to distinguish. However, the MS analysis revealed peptides unique to RTNLB5 and not RTNLB6, indicating that RTNLB5 was indeed detected. The role of this potential RTNLB5 interaction is unclear as RTNLB5 is mainly expressed in pollen (Arabidopsis eFP Browser, Winter et al., 2007) and involved in the karrikin response (Nelson et al., 2010). Thus, it is likely that RTNLB3 and RTNLB6 interact with each other in PD and are involved in the generation of the extremely fine ER-derived desmotubule (Knox et al., 2015). RTNLB1 is ubiquitously expressed in different tissues and developmental stages (Arabidopsis eFP Browser, Winter et al., 2007). Interestingly, it has been shown that a Serine-rich region in the N-terminal tail of RTNLB1, and also RTNLB2, interacts with the FLAGELLIN-SENSITIVE2 (FLS2) receptor (Lee et al., 2011). The double mutant rtnlb1/rtnlb2, as well as an RTNLB1-overexpressor, displayed reduced FLS2-dependent signalling and enhanced susceptibility to pathogen attacks (Lee et al., 2011). RTNLB1 and RTNLB2 may regulate FLS2-transport to the plasma membrane. FLS2 is localised at the plasma membrane, but also within PD (Monaghan and Zipfel, 2012), and may mediate the flg22-induced closure of PD (Faulkner et al., 2013).

d) Preference for PD and ER-localisation of the interaction candidates: The immunoprecipitation experiments identified several proteins present in the PD proteome, suggesting that RTNLB3 and RTNLB6 may be part of a protein complex within PD. We also found a number of PM-specific proteins that interacted with RTNLB3 and RTNLB6. Some of these proteins have a role in anchoring the ER to the PM. For example, SYTA is prevalent at ER-PM contact points in both animal cells (Giordano et al., 2013; Lin et al., 2014) and also in plant cells (Schapire et al., 2008; Yamazaki et al., 2010; Lewis and Lazarowitz, 2010; Uchiyama et al., 2014). Perez-Sancho et al. (2015) have suggested that SYTA on the PM may link the PM to the cortical ER conferring mechanotolerance at these points. However, they did not identify the interacting ER protein. Our current work suggests that RTNLBs on the cortical ER may perform such a linking function through a direct interaction with SYTA on the PM.

Another protein prevalent at ER-PM contact sites is VAP27 (Wang et al., 2014), also identified here as an interacting partner of RTNLB3 and RTNLB6. Recent studies suggest that a unique complex of proteins resides at such ER-PM contacts. VAP27 can bind microtubules and RTNLBs (current study), and also NET3c (Wang et al., 2014), a protein that links the actin cytoskeleton to the ER contacts. This protein complex may perform unique functions in anchoring and signalling between ER and PM (Wang et al., 2014). We suggest that the same complex may also function to anchor the desmotubule to the PM within or at the neck of the PD, perhaps explaining their prevalence in the PD proteome. SYTA is a Ca^{2+}-sensitive contractile protein (Yamazaki et al., 2010) that in the contracted form reduces the distance between adjacent membrane bi-layers to about 5 nm (Lin et al., 2014). PD closure is acutely sensitive to elevated Ca^{2+} levels (Tucker and Boss, 1996) and SYTA therefore emerges as a potential candidate for forcing the desmotubule and PM together upon Ca^{2+} influx. Significantly, like RTNLB3 and RTNLB6, SYTA appears in developing primary PD during cell-plate formation 2008) and remains associated with the entrances of mature PD (Schapire et al., 2008).

A number of the PD proteins that we found to interact with RTNLB3 and RTNLB6 are also the targets of viral MPs. These include SYTA (Lewis and Lazarowitz; Uchiyama et al., 2014), VAP27 (Carette et al., 2002), and the remorin proteins, remorin 1.2 and remorin 1.3 (Borner et al., 2005; Marin et al., 2012). A recent study (Levy et al., 2015) demonstrated that SYTA forms ER-PM junctions that are specifically recruited to PD during virus movement. Thus, proteins associated with the ER-PM contacts may be the specific targets of MPs during cell-cell movement. The association of these proteins with PD may provide a mechanism for targeting and concentrating viral genomes assembled on the actin-ER network and subsequently recruited to the entrances of PD (Tilsner et al., 2013; Levy et al., 2015). The PM intrinsic

protein, PIP3, functions as an aquaporin and is induced by salt-stress (Hachez et al., 2014a). The correct delivery of PIP3 to the PM involves specific interactions with two syntaxin proteins, SYP61 and SYP121 (Hachez et al., 2014b). PIP3 is also present in the PD proteome (Fernandez-Calvino et al., 2011), and via an interaction with RTNLBs may provide an additional link between the desmotubule and PM. TCP1 was pulled down only with RTNLB3 but not RTNLB6 and interacted only with RTNLB3 in FRET-FLIM assays. The TCP1 protein is part of a chaperonin complex involved in transcription factor trafficking through PD (Xu et al., 2011). One protein of this complex, CCT8, was shown recently to be required for Knotted1 trafficking through PD and is a target of the viral MP of TMV (Fichtenbauer et al., 2012). It appears that the entire chaperonin complex may be recruited for cell-cell trafficking (Xu et al., 2011). Conceivably, RTNLB3 provides a means of linking this complex to PD for the cell-cell movement of transcription factors.

In addition to proteins present at ER-PM contacts, our data reveal a number of PD proteins associated with lipid-rich domains in plants (Tapken and Murphy, 2015). This finding is in agreement with the view that PD are rich in lipid components (Naulin et al., 2014; Grison et al., 2015) and may function as unique lipid-rafts (Mongrand et al., 2010), perhaps involved in receptor-mediated signalling (Faulkner, 2013). The PM within PD is rich in sterols and sphingolipids relative to the general PM (Naulin et al., 2015). The PD-localised protein sterol methyltransferase SMT1 (AT5G13710) controls cholesterol levels (Diener et al., 2000), while the remorin proteins that interact with RTNLB3 and RTNLB6 are components of lipid rafts (Mongrand et al., 2010). Remorin 1.3 (REM1.3, AT2G45820) has been localised to PD *in planta* (Raffaele et al., 2009) and is differentially phosphorylated upon contact with bacterial elicitors. It may function as a scaffold protein in plant innate immunity (Benschop et al., 2007; Jarsch and Ott, 2011). The tomato REM1.3 is required for the restriction of potato virus X (PVX) trafficking (Perraki et al., 2012), while the potato Remorin1.3 affects the ability of the Triple Gene Block 1 (TGBp1) MP of PVX and other viral MPs to increase PD permeability (Perraki et al., 2014). Several remorins, including Arabidopsis REM1.3, form non-amyloid filamentous structures of 5.7 to 8.0 nm (Bariola et al., 2004; Marin et al., 2012). These remorins could be linked with the cytoskeleton in superstructures to maintain cell integrity, or act as scaffold proteins for signalling and defence mechanisms (Bariola et al., 2004), a process that might occur in combination with the structural RTNLB proteins.

Additional interacting proteins

DWARF1 (DWF1, AT3G19820) is a Ca2+-dependent calmodulin-binding protein involved in the conversion of the early brassinosteroid precursor 24-methylenecholesterol to campesterol. As brassinosteroids affect cellular elongation *dwf1* mutants display a dwarf phenotype due to

reduced cell expansion. Superroot 2 (SUR2, AT4G31500), catalyses the conversion of indole-3-acetaldoxime to indole-3-thiohydroxymate in indole glucosinolate biosynthesis (Barlier et al., 200; Bak et al., 2001) and was found here to interact with both RTNLB3 and RTNLB6. The biologically active degradation products of glucosinolates are formed under tissue disruption and are well known as the characteristic flavour compounds in mustard or cabbage (reviewed in Glawischnig et al., 2003). This could potentially link RTNLBs with defence mechanisms. DEFECTIVE GLYCOSYLATION (DGL1, AT5G66680) is a subunit of the ER oligosaccharyltransferase complex (Lerouxel et al., 2005). This protein complex is responsible for the transfer of N-linked glycan precursors onto Asn residues of candidate proteins in the ER. N-glycan synthesis pathways contribute to plant development as well as defence. The mutant *dgl1-1* displays developmental defects including reduced cell elongation and differentiation defects together with changes in the non-cellulosic matrix polysaccharides (Lerouxel et al., 2005).

Conclusions

Our combined experimental approach of using sensitive pulldown assays coupled with FRET-FLIM provides a robust means of identifying functional interactions for reticulon proteins. The primary MS dataset was validated using FRET-FLIM and showed that more than 80% of the candidate proteins were indeed interacting with the reticulons. The intermediate dataset was confirmed by a second set of proteomics data for both reticulons and confirmed both the proteomics as well as in particular the FRET-FLIM analysis indicating a high confidence for the final protein interactome.

Using two RTNLB proteins as bait, we have highlighted a significant number of PD proteins that interact with RTNLB3 and RTNLB6. We identified predominantly proteins associated with ER-PM contacts, proteins resident in lipid rafts and proteins that interact with viral MPs. These interaction studies will form the basis for future research aimed at unravelling the PD interactome. It will be interesting to determine which of these interactions are significant in regulating PD functions, such as the gating response that occurs during viral infection (Oparka et al., 1997).

Materials & Methods

Immunoprecipitation (GFP-Trap®_A beads)

Plant material for immunoprecipitation with the GFP-Trap®_A beads (Chromotek, Martinsried, Germany) was prepared according to the company's protocol with slight modifications.

In brief, approximately 5 g of whole seedling plant material grown for 2 weeks on MS plates were ground in liquid nitrogen and in lysis buffer (10 mM Tris-HCl pH 7.5, 150 mM NaCl; 0.5 mM EDTA, 0.5% NP-40, 1mM PMSF, protease inhibitor). The extracts were incubated on ice for 30 min and then centrifuged at 10,000g for 10 min at 4°C. The supernatant (about 2-3 ml) was poured into fresh tubes via 2 layers of muslin cloth.

The GFP-Trap®_A beads were equilibrated in 500µl dilution buffer (10 mM Tris-HCl pH 7.5, 150 mM NaCl, 0.5 mM EDTA) and centrifuged at 2,500 g for 2 min. The supernatant is being discarded and this wash is repeated twice.

100 µl of the washed beads were added to the plant extract and the mixture was shaken on ice for 2 hours. After this, tubes were centrifuged at 2,500 g for 2 min at 4°C, the supernatant discarded and the resulting agarose pellet was washed twice with dilution buffer.

Mass spectrometry (nanoLC-ESI-MS/MS) analysis

Reversed phase chromatography was used to separate tryptic peptides prior to MS analysis. Two columns were utilised, an Acclaim PepMap µ-precolumn cartridge 300 µm i.d. x 5 mm 5 µm 100 Å and an Acclaim PepMap RSLC 75 µm x 50 cm 2 µm 100 Å (Thermo Scientific). The columns were installed on an Ultimate 3000 RSLCnano system (Dionex). Mobile phase buffer A was composed of 0.1% aqueous formic acid and mobile phase B was composed of acetonitrile containing 0.1% formic acid. Samples were loaded onto the µ-precolumn equilibrated in 2% aqueous acetonitrile containing 0.1% trifluoroacetic acid for 8 min at 10 µL min^{-1} after which peptides were eluted onto the analytical column by increasing the mobile phase B concentration from 3% B to 35% over 87 min then to 90% B over 5 min, followed by a 4 min wash at 90% B and a 15 min re-equilibration at 3% B.

Eluting peptides were converted to gas-phase ions by means of electrospray ionization and analysed on a Thermo Orbitrap Fusion (Q-OT-qIT, Thermo Scientific). Survey scans of peptide precursors from 350 to 1500 *m*/*z* were performed at 120K resolution (at 200 *m*/*z*) with a 4×10^5 ion count target. Tandem MS was performed by isolation at 1.6 Th using the quadrupole, HCD fragmentation with normalized collision energy of 35, and rapid scan MS analysis in the ion trap. The MS^2 ion count target was set to 10^4 and the max injection time was 200 ms. Precursors with charge state 2–7 were selected and sampled for MS^2. The dynamic exclusion duration was set to 45 s with a 10 ppm tolerance around the selected

453 precursor and its isotopes. Monoisotopic precursor selection was turned on. The instrument
454 was run in top speed mode with 3 s cycles.
455
456 *Mass spectrometry data analysis*
457 Raw data was processed using MSConvert in ProteoWizard Toolkit (version 3.0.5759,
458 Kessner et al., 2008). MS^2 spectra were searched with Mascot engine (Matrix Science,
459 version 2.4.1) Mascot was set up to search the ArabidopsisTAIR10 database (version
460 20101214, 35508 entries) assuming the digestion enzyme trypsin. Mascot was searched with
461 a fragment ion mass tolerance of 0.80 Da and a parent ion tolerance of 20 PPM.
462 Carbamidomethyl of cysteine was specified in Mascot as a fixed modification. Oxidation of
463 methionine was specified in Mascot as a variable modification.
464 Scaffold (version Scaffold_4.4.1.1, Proteome Software Inc., Portland, OR) was used to
465 validate MS/MS based peptide and protein identifications. Peptide identifications were
466 accepted if they could be established at greater than 95.0% probability by the Scaffold Local
467 FDR algorithm. Protein identifications were accepted if they could be established at greater
468 than 99.0% probability and contained at least two identified peptides. Protein probabilities
469 were assigned by the Protein Prophet algorithm (Nesvizhskii et al., 2003). Proteins that
470 contained similar peptides and could not be differentiated based on MS/MS analysis alone
471 were grouped to satisfy the principles of parsimony.
472
473 *Cloning of expression plasmids*
474 Primers were obtained from MWG Biotech. Q5 high-fidelity DNA polymerase (New England
475 Biolabs) was used for all polymerase chain reaction reactions. Vectors containing the genes of
476 interest from the proteomics dataset were obtained from NASC (Scholl et al., 2000). Genes of
477 interest were cloned into the modified binary vectors pB7FWG2,0 or pB7WGR2,0 clone
478 providing expression from *Agrobacterium* T-DNA, using the cauliflower mosaic virus 35S
479 promoter upstream of coding fusions to green fluorescent protein (GFP) or red fluorescent
480 protein (RFP), respectively (Karimi et al., 2005).
481
482 *Tobacco plant material and transient expression in tobacco leaves*
483 For Agrobacterium-mediated transient expression, 5-week-old tobacco (*Nicotiana tabacum*
484 SR1 cv Petit Havana) plants grown in the greenhouse were used. Transient expression was
485 induced and detected according to Sparkes et al. (2006). In brief, each expression vector was
486 introduced into Agrobacterium strain GV3101 by heat shock. Transformants were inoculated
487 into 5 ml of YEB medium (5 g/l beef extract, 1 g/l yeast extract, 5 g/l sucrose and 0.5 g/l of
488 $MgSO_4 \cdot 7H_2O$) supplemented with the antibiotics for the vector and rifampicin to select for
489 agrobacteria. After overnight shaking at 25°C, 1 ml of the bacterial culture was pelleted by

centrifugation at 2,500×g for 5 min at room temperature. The pellet was washed twice with 1 ml of infiltration medium (50 mM MES, 2 mM $Na_3PO4 \cdot 12H_2O$, 0.1 mM acetosyringone and 5 mg/ml glucose) and then resuspended in 1 ml of infiltration buffer. The suspension was diluted to a final OD_{600} of 0.1 and gently pressed through the stomata on the lower epidermal surface using a 1 ml syringe. Transformed plants then were incubated under normal growth conditions for 48 to 72 h. Images were taken using a Zeiss LSM510 Meta laser scanning confocal microscope with a 63x oil immersion objective. For imaging of GFP/RFP combinations, samples were excited using 488 and 543 nm laser lines in multi-track mode with line switching. Images were edited using the LSM510 image browser.

FRET-FLIM data acquisition

Epidermal samples of infiltrated tobacco leaves were excised, and FRET-FLIM data capture was performed according to Osterrieder et al. (2009) and Schoberer and Botchway (2014) using a two-photon microscope at the Central Laser Facility of the Rutherford Appleton Laboratory. In brief, a two-photon microscope built around a Nikon TE2000-U inverted microscope was used with a modified Nikon EC2 confocal scanning system to allow for multiphoton FLIM, Botchway et al. (2015). Laser light at a wavelength of 920 nm was produced by a mode-locked titanium sapphire laser (Mira; Coherent Lasers), producing 200-fs pulses at 76 MHz, pumped by a solid-state continuous wave 532-nm laser (Verdi V18; Coherent Laser). The laser beam was focused to a diffraction-limited spot through a water immersion objective (Nikon VC x60, numerical aperture of 1.2) to illuminate specimens at the microscope stage. Fluorescence emission was collected without descanning, bypassing the scanning system, and passed through a BG39 (Comar) filter to block the near infrared laser light. Line, frame, and pixel clock signals were generated and synchronized with an external detector in form of a fast microchannel plate photomultiplier tube (MCP-PMT; Hamamatsu R3809U). Linking these via a time-correlated single-photon-counting PC module SPC830 (Becker and Hickl) generated the raw FLIM data. Prior to FLIM data collection, the GFP and mRFP expression levels in the plant samples within the region of interest were confirmed using a Nikon EC2 confocal microscope with excitation at 488 and 543 nm, respectively. A 633-nm interference filter was used to significantly minimize the contaminating effect of chlorophyll autofluorescence emission that would otherwise obscure the mRFP emission as well as that of GFP. Data were analyzed by obtaining excited state lifetime values of a region of interest on the nucleus, and calculations were made using the SPCImage analysis software version 5.1 (Becker and Hickl). The distribution of lifetime values within the ROI were generated and displayed as a curve. Only values that had a χ^2 between 0.9 and 1.4 were taken. The median lifetime value and minimum and maximum values for a quarter of the

median lifetime values from the curve were taken to generate the range of lifetimes per sample.

At least three nuclei from at least three independent biological samples per protein-protein combination were analyzed, and the average of the ranges taken.

Accession Numbers

Sequence data for genes in this article can be found in GenBank/EMBL databases using the following accession numbers: RTNLB3, At1g64090 and RTNLB6, At3g61560. All access numbers from the proteomic analysis can be found in the corresponding tables.

Author Contributions

V.K, K.O, and C.H designed the research. V.K and S.S performed the research. V.K, S.B, S.S, K.O and C.H analysed the data. All authors contributed to the writing of the paper.

Tables

Table 1: Analysis steps and number of proteins derived from mass spec analysis.

Analysis Step	N° of proteins
Total (RTNLB3/RTNLB6)	706 (613/621)
Minus WT control total (RTNLB3/RTNLB6)	146 (135/126)
Proteins subjected to FRET-FLIM analysis	17

Table 2: Flowchart of the 17 proteins tested by FRET-FLIM with protein description (column 1) and accession number (column 2) indicating their % abundance in the total spectrum for RTNLB3 (column 3) or RTNLB6 (column 4), respectively. Proteins present in the PD proteome (Fernandez-Calvino et al., 2011) are marked with an asterisk. Positive (+) or negative (-) results for interaction in the FRET-FLIM analysis with either RTNLB3 (column 5) or RTNLB6 (column 6) are shown. The re-appearance of the corresponding protein in the second MS run is shown (RTNLB3-2 and RTNLB6-2, column 7 and 8).

		% in total spectra			FRET-FLIM			present in 2nd MS run	
Proteins	Accession No	RTNLB3-1	RTNLB6 -1		RTNLB3-1	RTNLB6 -1		RTNLB3-2	RTNLB6 -2
Reticulan like protein RTNLB3 *	AT1G64090.1	0.042%	0.036%		+	+		+	+
Reticulon family protein RTNLB6 *	AT3G61560.1	0.019%	0.170%		+	+		+	+
SYTA, SYT1 | synaptotagmin A *	AT2G20990.1	0.032%	0.081%		+	+		+	+
Root hair defective 3 GTP-binding protein (RHD3)	AT3G13870.1	0.019%	0.052%		+	+		+	+
DWF1, DIM, EVE1, DIM1, CBB1 | cell elongation protein	AT3G19820.1	0.023%	0.036%		+	+		+	+
DGL1 | dolichyl-diphosphooligosaccharide-protein glycosyltransferase *	AT5G66680.1	0.013%	0.023%	FRET-FLIM	+	+	2nd MS run	+	+
ATB5-B, B5 #3, ATCB5-D, CB5-D | cytochrome B5 isoform D	AT5G48810.1	0.013%	0.019%		+	+		+	+
SMT1, CPH | sterol methyltransferase 1 *	AT5G13710.1	0.003%	0.013%		+	+		+	+
CYP83B1, SUR2, RNT1, RED1, ATR4 | cytochrome P450, family 83	AT4G31500.1	0.010%	0.013%		+	+		+	+
PIP3, PIP3A, PIP2;7, SIMIP | plasma membrane intrinsic protein 3 *	AT4G35100.1	0.010%	0.013%		+	+		+	+
Remorin family protein REM1.3 *	AT2G45820.1	0.010%	0.010%		+	+		+	+
Remorin family protein REM1.2 *	AT3G61260.1	0.013%	0.010%		+	+		+	+
FLA8, AGP8 | FASCICLIN-like arabinogalactan protein 8 *	AT2G45470.1	0.007%	0.010%		-	-		-	-
VAP27-1, VAP, (AT)VAP, VAP27 | vesicle associated protein	AT3G60600.1	0.007%	0.007%		+	+		+	+
ANNAT4 | annexin 4 *	AT2G38750.1	0.010%	0.007%		-	-		-	-
ATTRX3, ATH3, ATTRXH3, TRXH3, TRX3 | thioredoxin 3 *	AT5G42980.1	0.007%	0.003%		-	-		-	-
TCP-1/cpn60 chaperonin family protein *	AT3G03960.1	0.013%	0.000%		+	-		+	-

Table 3: Fluorescent lifetimes in FRET-FLIM analysis. Donor and acceptor protein constructs are indicated together with the average fluorescent lifetime in ns for the donor fluorophore and the standard deviation for each combination. It was previously shown that a reduction in excited state lifetime of 200 ps is indicative to energy transfer (Stubbs et al., 2005). For each combination at least two biological samples with a minimum of three technical replicates were used for the statistical analysis.

Donor (GFP)		Acceptor (mRFP)	Average [ns]	Std error
RTNLB3	+	(-)	2.51	0.05
RTNLB3	+	RTNLB3	2.28	0.01
RTNLB3	+	RTNLB6	2.31	0.01
RTNLB3	+	SYTA	2.29	0.04
RTNLB3	+	RHD3	2.30	0.01
RTNLB3	+	DWF1	2.28	0.01
RTNLB3	+	DGL1	2.37	0.01
RTNLB3	+	Cyb5D	2.30	0.01
RTNLB3	+	SMT1	2.29	0.03
RTNLB3	+	SUR2	2.28	0.06
RTNLB3	+	PIP3	2.37	0.02
RTNLB3	+	REM1.3	2.33	0.02
RTNLB3	+	REM1.2	2.31	0.01
RTNLB3	+	FLA8	2.53	0.09
RTNLB3	+	Vap27	2.33	0.03
RTNLB3	+	ANNAT4	2.50	0.03
RTNLB3	+	TRX3	2.48	0.03
RTNLB3	+	TCP1	2.32	0.01

Donor (GFP)		Acceptor (mRFP)	Average [ns]	Std error
RTNLB6	+	(-)	2.63	0.06
RTNLB6	+	RTNLB3	2.37	0.04
RTNLB6	+	RTNLB6	2.38	0.01
RTNLB6	+	SYTA	2.46	0.02
RTNLB6	+	RHD3	2.34	0.01
RTNLB6	+	DWF1	2.32	0.01
RTNLB6	+	DGL1	2.37	0.07
RTNLB6	+	Cyb5D	2.47	0.02
RTNLB6	+	SMT1	2.36	0.07
RTNLB6	+	SUR2	2.34	0.11
RTNLB6	+	PIP3	2.35	0.04
RTNLB6	+	REM1.3	2.44	0.05
RTNLB6	+	REM1.2	2.48	0.01
RTNLB6	+	FLA8	2.67	0.07
RTNLB6	+	Vap27	2.33	0.04
RTNLB6	+	ANNAT4	2.66	0.03
RTNLB6	+	TRX3	2.62	0.06
RTNLB6	+	TCP1	2.60	0.02

Table 4: List of interacting proteins for RTNLB3 (top) and RTNLB6 (bottom), respectively, present in both MS datasets. The protein name, accession number and molecular weight (MW) are given. The percentage of the total spectra in both MS datasets (MS run1 and 2) is given as well as known or predicted subcellular localisation for plasmodesmata (PD, yellow), ER (blue), plasma membrane (PM, green) or cell plate (purple). More detail for the interacting proteins can be found in Supplemental Table 2.

RTNLB3: interacting proteins	*Accession number*	*MW*	*MS run1*	*MS run2*	*Subcellular localisation*			
			RTN3-1	RTN3-2	PD	ER	PM	Cell plate
SYTA, NTMC2TYPE1.1, ATSYTA, NTMC2T1.1, SYT1 synaptotagmin A	AT2G20990.1	62 kDa	0.066%	0.032%	+		+	
RTNLB3 Reticulan like protein B3	AT1G64090.2	31 kDa	0.058%	0.039%	+	+		
RTNLB3 Reticulan like protein B3	AT1G64090.1	29 kDa	0.042%	0.036%	+	+		
SYTA synaptotagmin A, SYT1	AT2G20990.3	66 kDa	0.032%	0.081%	+		+	
ATC4H, C4H, CYP73A5, REF3 cinnamate-4-hydroxylase	AT2G30490.1	58 kDa	0.029%	0.049%	+	+		
ERD4 Early-responsive to dehydration stress protein (ERD4)	AT1G30360.1	82 kDa	0.026%	0.013%	+		+	
DWF1, DIM, EVE1, DIM1, CBB1 cell elongation protein	AT3G19820.1	65 kDa	0.023%	0.036%		+	+	
Reticulon family protein RTNLB6	AT3G61560.1	29 kDa	0.019%	0.170%	+	+		
RHD3 Root hair defective 3 GTP-binding protein	AT3G13870.1	89 kDa	0.019%	0.052%		+		
ATB5-A, B5 #2, ATCB5-E, CB5-E cytochrome B5 isoform E	AT5G53560.1	15 kDa	0.019%	0.026%		+		
LACS4 AMP-dependent synthetase and ligase family protein	AT4G23850.1	75 kDa	0.016%	0.019%			+	
DGL1 dolichyl-diphosphooligosaccharide-protein glycosyltransferase	AT5G66680.1	49 kDa	0.013%	0.023%	+	+	+	
CYP71B7 cytochrome P450, family 71 subfamily B, polypeptide 7	AT1G13110.1	57 kDa	0.013%	0.019%			+	
ATB5-B, B5 #3, ATCB5-D, CB5-D cytochrome B5 isoform D	AT5G48810.1	15 kDa	0.013%	0.019%		+		
Remorin family protein	AT3G61260.1	23 kDa	0.013%	0.010%	+		+	
ADL1, ADL1A, AG68, DRP1A, RSW9, DL1 dynamin-like protein	AT5G42080.1	68 kDa	0.013%	0.010%				+
TCP-1/cpn60 chaperonin family protein	AT3G03960.1	59 kDa	0.013%	0.010%	+			
ATRAB11A, ATRABA2C, ATRAB-A2C, RAB-A2C	AT3G46830.1	24 kDa	0.010%	0.026%			+	+
catalytics	AT5G11560.1	109 kDa	0.010%	0.016%		+	+	
CYP83B1, SUR2, RNT1, RED1, ATR4 cytochrome P450, family 83	AT4G31500.1	57 kDa	0.010%	0.013%		+		
PIP3, PIP3A, PIP2;7, SIMIP plasma membrane intrinsic protein 3	AT4G35100.1	30 kDa	0.010%	0.013%	+		+	
ATCBR, CBR1, CBR NADH:cytochrome B5 reductase 1	AT5G17770.1	31 kDa	0.010%	0.013%		+	+	
Remorin family protein	AT2G45820.1	21 kDa	0.010%	0.010%	+		+	
unknown protein, protein family UPF0121	AT3G02420.1	40 kDa	0.010%	0.010%	+	+		
SOUL-1 AtHBP2/ SOUL heme-binding family protein	AT2G37970.1	25 kDa	0.010%	0.007%				
SMT2, CVP1, FRL1 sterol methyltransferase 2	AT1G20330.1	40 kDa	0.007%	0.023%		+		
BTI1, RTNLB1 VIRB2-interacting protein 1	AT4G23630.1	31 kDa	0.007%	0.019%		+		
ATJ3, ATJ DNAJ homologue 3	AT3G44110.1	46 kDa	0.007%	0.013%	+			
FAH1, CYP84A1 ferulic acid 5-hydroxylase 1	AT4G36220.1	59 kDa	0.007%	0.010%		+		
VAP27-1, VAP, (AT)VAP, VAP27 vesicle associated protein	AT3G60600.1	28 kDa	0.007%	0.003%		+		
SHD, HSP90.7, AtHsp90.7, AtHsp90-7 Chaperone protein htpG family protein	AT4G24190.1	94 kDa	0.007%	0.003%		+		
Ribosomal protein S8e family protein	AT5G20290.1	25 kDa	0.007%	0.003%		+		
NTMC2TYPE4, NTMC2T4 Calcium-dependent lipid-binding family protein	AT3G61050.1	55 kDa	0.003%	0.029%		+	+	
Reticulon family protein RTNLB5	AT2G46170.1	29 kDa	0.003%	0.023%		+		
RHD4 Phosphoinositide phosphatase family protein	AT3G51460.1	68 kDa	0.003%	0.016%	+	+	+	
GPAT8, AtGPAT8 glycerol-3-phosphate acyltransferase 8	AT4G00400.1	56 kDa	0.003%	0.016%		+		
Endomembrane protein 70 protein family	AT5G25100.1	74 kDa	0.003%	0.016%			+	
SMT1, CPH sterol methyltransferase 1	AT5G13710.1	38 kDa	0.003%	0.013%	+	+		
RAB11, ATRABA1B, RABA1b RAB GTPase homolog A1B	AT1G16920.1	24 kDa	0.003%	0.007%			+	
Ribophorin I	AT2G01720.1	52 kDa	0.003%	0.007%		+	+	
Endomembrane protein 70 protein family	AT2G01970.1	68 kDa	0.003%	0.007%			+	
PHOT1, NPH1, JK224, RPT1 phototropin 1	AT3G45780.1	112 kDa	0.003%	0.007%			+	

RTNLB6: interacting proteins	*Accession number*	*MW*	*MS run1*	*MS run2*	*Subcellular localisation*			
			RTN6-1	RTN6-2	PD	ER	PM	Cell plate
Reticulon family protein RTNLB6	AT3G61560.1	29 kDa	0.019%	0.170%	+	+		
SYTA, NTMC2TYPE1.1, ATSYTA, NTMC2T1.1, SYT1 synaptotagmin A	AT2G20990.1	62 kDa	0.032%	0.081%	+		+	
SYTA synaptotagmin A, SYT1	AT2G20990.3	66 kDa	0.032%	0.081%	+	+		
RHD3 Root hair defective 3 GTP-binding protein	AT3G13870.1	89 kDa	0.019%	0.052%		+		
ATC4H, C4H, CYP73A5, REF3 cinnamate-4-hydroxylase	AT2G30490.1	58 kDa	0.029%	0.049%	+	+		
FUNCTIONS IN: molecular_function unknown	AT2G32240.1	?	0.052%	0.039%			+	
RTNLB3 Reticulan like protein B3	AT1G64090.1	29 kDa	0.042%	0.036%	+	+		
DWF1, DIM, EVE1, DIM1, CBB1 cell elongation protein	AT3G19820.1	65 kDa	0.023%	0.036%		+	+	
CCD1, ATCCD1, ATNCED1, NCED1 carotenoid cleavage dioxygenase 1	AT3G63520.1	61 kDa	0.023%	0.029%	+		+	
NTMC2TYPE4, NTMC2T4 Calcium-dependent lipid-binding family protein	AT3G61050.1	55 kDa	0.003%	0.029%		+	+	
ALDH3F1 aldehyde dehydrogenase 3F1	AT4G36250.1	54 kDa	0.000%	0.029%		+		
DGL1 dolichyl-diphosphooligosaccharide-protein glycosyltransferase	AT5G66680.1	49 kDa	0.013%	0.023%	+	+	+	
SMT2, CVP1, FRL1 sterol methyltransferase 2	AT1G20330.1	40 kDa	0.007%	0.023%		+		
Reticulon family protein RTNLB3	AT2G46170.1	29 kDa	0.003%	0.023%		+		
LACS4 AMP-dependent synthetase and ligase family protein	AT4G23850.1	75 kDa	0.016%	0.019%			+	
CYP71B7 cytochrome P450, family 71 subfamily B, polypeptide 7	AT1G13110.1	57 kDa	0.013%	0.019%			+	
ATB5-B, B5 #3, ATCB5-D, CB5-D cytochrome B5 isoform D	AT5G48810.1	15 kDa	0.013%	0.019%		+		
BTI1, RTNLB1 VIRB2-interacting protein 1	AT4G23630.1	31 kDa	0.007%	0.019%		+		
Eukaryotic aspartyl protease family protein	AT1G03220.1	46 kDa	0.032%	0.016%	+		+	
MO1 monooxygenase 1	AT4G15760.1	47 kDa	0.023%	0.016%		+		
APX3 ascorbate peroxidase 3	AT4G35000.1	32 kDa	0.019%	0.016%		+		
UCC2 uclacyanin 2	AT2G44790.1	20 kDa	0.016%	0.016%	+		+	
catalytics	AT5G11560.1	109 kDa	0.010%	0.016%		+	+	
RHD4 Phosphoinositide phosphatase family protein	AT3G51460.1	68 kDa	0.003%	0.016%	+	+	+	
Endomembrane protein 70 protein family	AT5G25100.1	74 kDa	0.003%	0.016%			+	
ERD4 Early-responsive to dehydration stress protein (ERD4)	AT1G30360.1	82 kDa	0.026%	0.013%	+		+	
CYP83B1, SUR2, RNT1, RED1, ATR4 cytochrome P450, family 83	AT4G31500.1	57 kDa	0.010%	0.013%		+		
PIP3, PIP3A, PIP2;7, SIMIP plasma membrane intrinsic protein 3	AT4G35100.1	30 kDa	0.010%	0.013%	+		+	
CYP71B6 cytochrome p450 71b6	AT2G24180.1	57 kDa	0.007%	0.013%		+	+	
Carbohydrate-binding-like fold	AT3G62360.1	133 kDa	0.007%	0.013%		+	+	
ALDH22A1 aldehyde dehydrogenase 22A1	AT3G66658.2	66 kDa	0.007%	0.013%		+		
SMT1, CPH sterol methyltransferase 1	AT5G13710.1	38 kDa	0.003%	0.013%	+	+		
Remorin family protein	AT3G61260.1	23 kDa	0.013%	0.010%	+		+	
Remorin family protein	AT2G45820.1	21 kDa	0.010%	0.010%	+		+	
unknown protein, protein family UPF0121	AT3G02420.1	40 kDa	0.010%	0.010%	+	+		
Protein of unknown function DUF2359, transmembrane	AT1G70770.1	67 kDa	0.007%	0.010%		+	+	
FAH1, CYP84A1 ferulic acid 5-hydroxylase 1	AT4G36220.1	59 kDa	0.007%	0.010%		+		
ATPDIL5-2, ATPDI8, PDI8, PDIL5-2 PDI-like 5-2	AT1G35620.1	50 kDa	0.003%	0.010%	+	+		
Endomembrane protein 70 protein family	AT4G12650.1	74 kDa	0.003%	0.010%	+			
Saccharopine dehydrogenase	AT5G39410.1	50 kDa	0.003%	0.010%			+	
VAP27-1, VAP, (AT)VAP, VAP27 vesicle associated protein	AT3G60600.1	28 kDa	0.007%	0.007%		+		
STL2P, ATSEC12 SEC12P-like 2 protein	AT2G01470.1	43 kDa	0.010%	0.007%		+		
ALDH3H1, ALDH4 aldehyde dehydrogenase 3H1	AT1G44170.1	53 kDa	0.007%	0.007%	+	+		
ATRAB11C, ATRABA2A, ATRAB-A2A, RAB-A2A,	AT1G09630.1	24 kDa	0.003%	0.007%			+	+
RAB11, ATRABA1B, RABA1b RAB GTPase homolog A1B	AT1G16920.1	24 kDa	0.003%	0.007%			+	
Endomembrane protein 70 protein family	AT2G01970.1	68 kDa	0.003%	0.007%			+	
Protein of unknown function (DUF3754)	AT3G19340.1	57 kDa	0.003%	0.007%			+	
PHOT1, NPH1, JK224, RPT1 phototropin 1	AT3G45780.1	112 kDa	0.003%	0.007%			+	
Leucine-rich repeat protein kinase family protein	AT5G49760.1	105 kDa	0.003%	0.007%			+	
Oligosaccharyltransferase complex/magnesium transporter family protein	AT1G61790.1	39 kDa	0.000%	0.007%		+	+	
Calcium-dependent phosphotriesterase superfamily protein	AT3G57030.1	41 kDa	0.000%	0.007%		+	+	
SQS1, ERG9 squalene synthase 1	AT4G34640.1	47 kDa	0.000%	0.007%		+	+	
ATPLC2, PLC2 phospholipase C 2	AT3G08510.1	66 kDa	0.010%	0.003%			+	
Clathrin light chain protein	AT2G20760.1	37 kDa	0.007%	0.003%			+	
ATMIN7, BEN1 HOPM interactor 7	AT3G43300.1	195 kDa	0.007%	0.003%				
SHD, HSP90.7, AtHsp90.7, AtHsp90-7 Chaperone protein htpG	AT4G24190.1	94 kDa	0.007%	0.003%		+		
ATBAG7, BAG7 BCL-2-associated athanogene 7	AT5G62390.1	52 kDa	0.007%	0.003%		+		

572

573

Figure Legends

Figure 1

Quantitative scatterplot for overlay and distribution of candidate interaction proteins for RTNLB3 and RTNLB6 (Scaffold_4.4.1.1 Proteome Software). Each protein is plotted as a point on a two dimensional scatterplot with the X-axis showing a normalized spectral count for proteins binding to RTLB3 and the Y-axis for RTNLB6. The Scaffold software shows a line with a slope of 1 on the graph. Therefore proteins with similar abundances in both co-immunoprecipitation assays will plot as points near this line. Proteins that plot outside the indicated dashed lines on the plot are more than two standard deviations away from being the same in both co-immunoprecipitation. These proteins are considered to be differentially expressed.

Figure 2

FRET-FLIM analysis of RTNLB6 without an interaction partner (**A-D**) or RTNLB6 dimerization (**E-I**). Images A and E display the raw FRET-FLIM data. In **B** and **F** pseudo-coloured lifetime maps show the lifetime values for each point within the region of interest while the distribution of lifetimes across the entire image is shown in **C** and **G** with blue shades representing longer GFP-fluorescence lifetimes than green ones. Images **D** and **H** display representative decay curves of a single point with an optimal single exponential fit, where Chi square (χ^2) values from 0.9 to 1.2 were considered an excellent fit to the data points (binning factor of 2. Images **A** (inset) and **I** are the respective confocal images for the analysis showing the GFP-construct in green and the mRFP-construct in red. This example of FRET-FLIM analysis shows that RTNLB6 homodimerizes because the lifetime values for the GFP/mRFP fusion pair (image H, 2.38±0.01 ns) are lower than those for the GFP fusion alone (image D, 2.63±0.06 ns). White bar = 5µm.

Figure 3

Fluorescent lifetimes in FRET-FLIM interactions. The bar graph represents average fluorescent lifetimes [ns] and the corresponding standard deviations for the GFP-donors RTNLB3 and RTNLB6, respectively. The data show 17 candidate interaction proteins (blue bars) compared to RTNLB3-GFP or RTNLB6-GFP without interaction partners (grey bars). Lifetimes significantly lower than those of RTNLB3-GFP or RTNLB6-GFP alone (left hand side of the red line) indicate protein-protein interactions.

Figure 4

610 Quantitative distribution (%) of predicted or known subcellular localisations for RTNLB3 and
611 RTNLB6 interaction candidates validated by two MS datasets and FRET-FLIM.

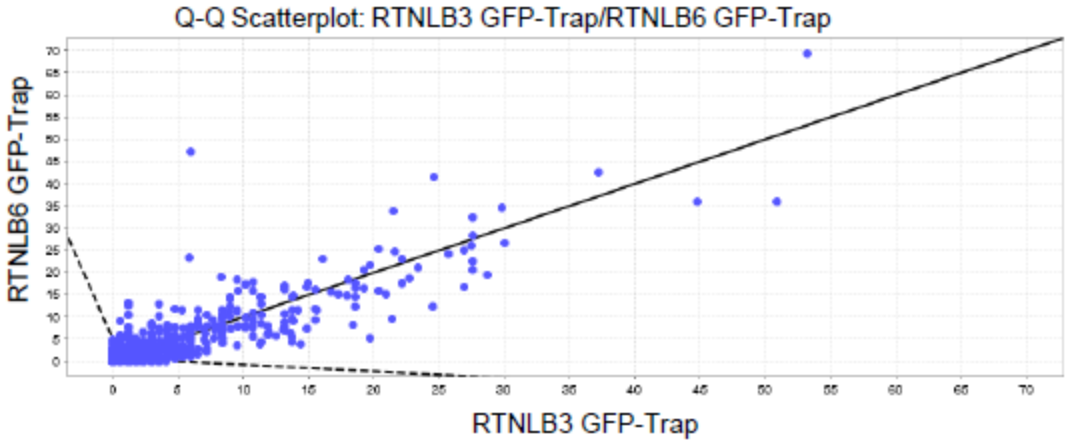

Figure 1
Quantitative scatterplot for overlay and distribution of candidate interaction proteins for RTNLB3 and RTNLB6 (Scaffold_4.4.1.1 Proteome Software).Each protein is plotted as a point on a two dimensional scatterplot with the X-axis showing a normalized spectral count for proteins binding to RTLB3 and the Y-axis for RTNLB6. The Scaffold software shows a line with a slope of 1 on the graph. Therefore proteins with similar abundances in both co-immunoprecipitation assays will plot as points near this line. Proteins that plot outside the indicated dashed lines on the plot are more than two standard deviations away from being the same in both co-immunoprecipitation. These proteins are considered to be differentially expressed.

612

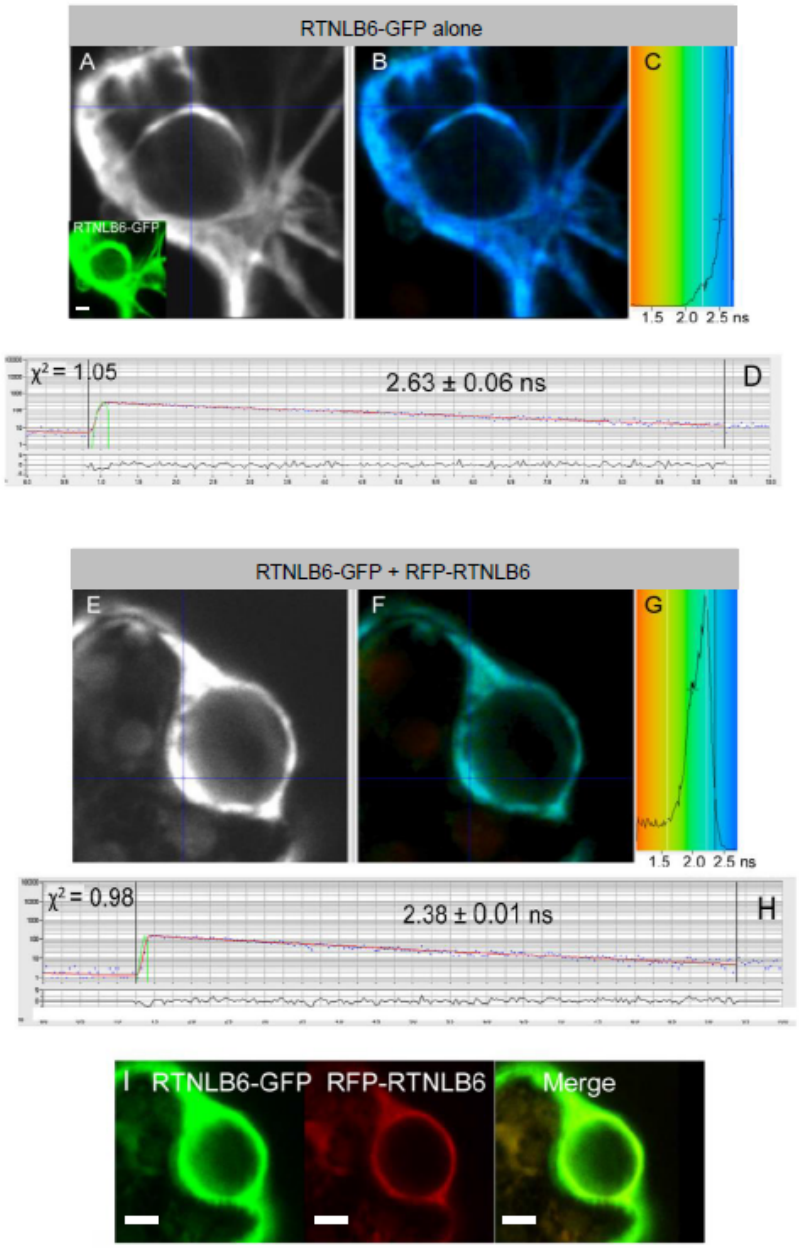

Figure 2

FRET-FLIM analysis of RTNLB6 without an interaction partner (**A-D**) or RTNLB6 dimerization (**E-I**). Images A and E display the raw FRET-FLIM data. In **B** and **F** pseudo-coloured lifetime maps show the lifetime values for each point within the region of interest while the distribution of lifetimes across the entire image is shown in **C** and **G** with blue shades representing longer GFP-fluorescence lifetimes than green ones. Images **D** and **H** display representative decay curves of a single point with an optimal single exponential fit, where Chi square (χ^2) values from 0.9 to 1.2 were considered an excellent fit to the data points (binning factor of 2. Images **A** (inset) and **I** are the respective confocal images for the analysis showing the GFP-construct in green and the mRFP-construct in red. This example of FRET-FLIM analysis shows that RTNLB6 homodimerizes because the lifetime values for the GFP/mRFP fusion pair (image H, 2.38±0.01 ns) are lower than those for the GFP fusion alone (image D, 2.63±0.06 ns). White bar = 5µm.

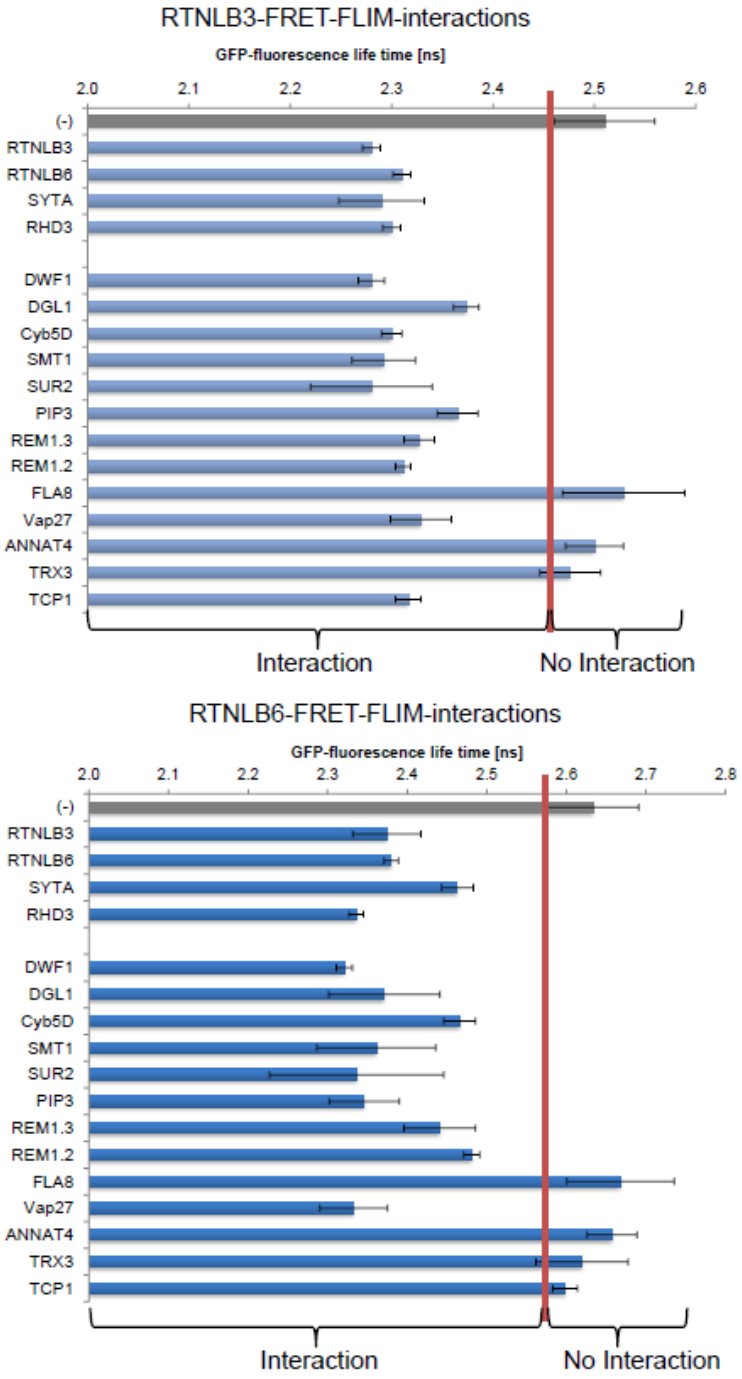

Figure 3

Fluorescent lifetimes in FRET-FLIM interactions. The bar graph represents average fluorescent lifetimes [ns] and the corresponding standard deviations for the GFP-donors RTNLB3 and RTNLB6, respectively. The data show 17 candidate interaction proteins (blue bars) compared to RTNLB3-GFP or RTNLB6-GFP without interaction partners (grey bars). Lifetimes significantly lower than those of RTNLB3-GFP or RTNLB6-GFP alone (left hand side of the red line) indicate protein-protein interactions.

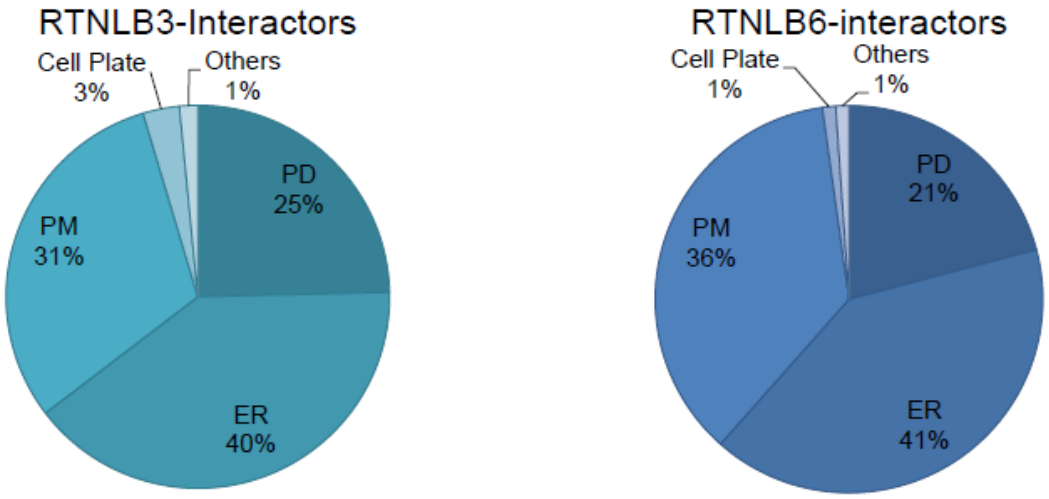

Figure 4
Quantitative distribution (%) of predicted or known subcellular localisations for RTNLB3 and RTNLB6 interaction candidates validated by two MS datasets and FRET-FLIM.

615

References

Bariola PA, Retelska D, Stasiak A, Kammerer RA, Fleming A, Hijri M, Frank S, Farmer EE (2004) Remorins form a novel family of coiled coil-forming oligomeric and filamentous proteins associated with apical, vascular and embryonic tissues in plants. *Plant Mol Biol* **55**: 579–594

Barlier I, Kowalczyk M, Marchant A, Ljung K, Bhalerao R, Bennett M, Sandberg G, Bellini C (2000) The SUR2 gene of Arabidopsis thaliana encodes the cytochrome P450 CYP83B1, a modulator of auxin homeostasis. *Proc Natl Acad Sci USA* **97**: 14819–14824

Bak S, Tax FE, Feldmann KA, Galbraith DW, Feyereisen R (2001) CYP83B1, a cytochrome P450 at the metabolic branch point in auxin and indole glucosinolate biosynthesis in Arabidopsis. *Plant Cell* **13**: 101–111

Bayer EM, Mongrand S, Tilsner J (2014) Specialized membrane domains of plasmodesmata, plant intercellular nanopores. *Front Plant Sci* **30**(5): 507

Beck M, Heard W, Mbengue M, Robatzek S (2012) The INs and OUTs of pattern recognition receptors at the cell surface. *Curr Opin Plant Biol* **15**(4): 367–74

Becker W (2012) Fluorescence lifetime imaging-techniques and applications. *J Microsc* **247**: 119–136

Benschop JJ, Mohammed S, O'Flaherty M, Heck AJ, Slijper M, Menke FL (2007) Quantitative phosphoproteomics of early elicitor signalling in *Arabidopsis. Mol Cell Proteomics* **6**: 1198–1214

Bernard A, Domergue F, Pasca, S, Jetter,R, Renne C, Faure JD, Haslam RP, Napier JA, Lessire R, Joubès J (2012) Reconstitution of Plant Alkane Biosynthesis in Yeast Demonstrates That Arabidopsis ECERIFERUM1 and ECERIFERUM3 Are Core Components of a Very-Long-Chain Alkane Synthesis Complex. *The Plant Cell* **24**: 3106–3118

Borner GH, Sherrier DJ, Weimar T, Michaelson LV, Hawkins ND, Macaskill A, Napier JA, Beale MH, Lilley KS, Dupree P (2005) Analysis of detergent-resistant membranes in *Arabidopsis* Evidence for plasma membrane lipid rafts. *Plant Physiol* **137**(1): 104–116

652 Botchway SW, Scherer KM, Hook S, Stubbs CD, Weston E, Bisby RH, Parker AW (2015) A
653 series of flexible design adaptations to the Nikon E-C1 and E-C2 confocal microscope
654 systems for UV, multiphoton and FLIM imaging. *J Microsc* **258**(1): 68–78
655
656 Carette JE, Verver J, Martens J, van Kampen T, Wellink J, van Kammen A (2002)
657 Characterization of plant proteins that interact with cowpea mosaic virus '60K' protein in the
658 yeast two-hybrid system. *J Gen Virol* **83**(Pt 4): 885–93
659
660 Chang J, Clay JM, Chang C (2014) Association of cytochrome b5
661 with ETR1 ethylene receptor signaling through RTE1 in Arabidopsis. *Plant J* **77**(4): 558–67
662
663 Clouse SD (2000) Plant development: A role for sterols in embryogenesis. *Curr Biol* **24**;10(16):
664 R601–4
665
666 Diener AC, Li H, Zhou W, Whoriskey WJ, Nes WD, Fink GR (2000)
667 Sterol methyltransferase 1 controls the level of cholesterol in plants. *Plant Cell* **12**(6): 853–70
668
669 Ehlers K, Kollmann R (2001) Primary and secondary plasmodesmata: structure, origin and
670 functioning. *Protoplasma* **216**: 1–30
671
672 Faulkner C, Petutschnig E, Benitez-Alfonso Y, Beck M, Robatzek S, Lipka V, Maule AJ (2013)
673 LYM2-dependent chitin perception limits molecular flux via plasmodesmata. *Proc Natl Acad*
674 *Sci U S A* **110**(22): 9166–70
675
676 Giordano F, Saheki Y, Idevall-Hagren O, Colombo SF, Pirruccello M, Milosevic I, Gracheva
677 EO, Bagriantsev SN, Borgese N, De Camilli P (2013) PI(4,5)P(2)-dependent and Ca(2+)-
678 regulated ER-PM interactions mediated by the extended synaptotagmins. *Cell* **20**;153(7):
679 1494–509
680
681 Grison MS, Brocard L, Fouillen L, Nicolas W, Wewer V, Dörmann P, Nacir H, Benitez-Alfonso
682 Y, Claverol S, Germain V, Boutté Y, Mongrand S, Bayer EM (2015) Specific membrane lipid
683 composition is important for plasmodesmata function in Arabidopsis. *Plant Cell* **27**(4): 1228–
684 50
685
686 Fernandez-Calvino L, Faulkner C, Walshaw J, Saalbach G, Bayer E, Benitez-Alfonso Y,
687 Maule A (2011) Arabidopsis plasmodesmal proteome. *PLoS One* **6**(4):e18880
688

689 Fichtenbauer D, Xu XM, Jackson D, Kragler F (2012) The chaperonin CCT8 facilitates spread
690 of tobamovirus infection. *Plant Signal Behav* **7**(3): 318–21
691
692 Förster T (1948) Zwischenmolekulare Energiewanderung und Fluoreszenz. *Ann Phys* **437**:
693 55–75
694
695 Glawischnig E, Mikkelsen MD, Halkier BA (2003) Glucosinolates: Biosynthesis and
696 Metabolism. Y Abrol, A Ahmad eds, Sulphur in plants. Kluwer Academic Publishers,
697 Dordrecht, The Netherlands: 145–162
698
699 Hachez C, Veljanovski V, Reinhardt H, Guillaumot D, Vanhee C, Chaumont F, Batoko H
700 (2014a) The *Arabidopsis* Abiotic Stress-Induced TSPO-Related Protein Reduces Cell-Surface
701 Expression of the Aquaporin PIP2;7 through Protein-Protein Interactions and Autophagic
702 Degradation. *Plant Cell* **26**(12): 4974–90
703
704 Hachez C, Laloux T, Reinhardt H, Cavez D, Degand H, Grefen C, De Rycke R, Inzé D, Blatt M
705 R, Russinova E, Chaumont F (2014b) Arabidopsis SNAREs SYP61 and SYP121 Coordinate
706 the Trafficking of Plasma Membrane Aquaporin PIP2;7 to Modulate the Cell Membrane Water
707 Permeability. *Plant Cell* **26**(7): 3132–47
708
709 Hawes C, Kiviniemi P, Kriechbaumer V (2015) The endoplasmic reticulum: a dynamic and
710 well-connected organelle. *J Integr Plant Biol* **57**(1): 50–62
711
712 Hu J, Shibata Y, Voss C, Shemesh T, Li Z, Coughlin M, Kozlov MM, Rapoport TA, Prinz WA
713 (2008) Membrane proteins of the endoplasmic reticulum induce high-curvature tubules.
714 *Science* **319**: 1247–1250
715
716 Jarsch IK, Ott T (2011) Perspectives on remorin proteins, membrane rafts, and their role
717 during plant-microbe interactions. *Mol Plant Microbe Interact* **24**: 7–12
718
719 Karimi M, De Meyer B, Hilson P (2005) Molecular cloning and expression of tagged
720 fluorescent protein in plant cells. *Trends Plant Sci* **10**: 103–105
721
722 Kessner D, Chambers M, Burke R, Agus D, Mallick P (2008) ProteoWizard: open source
723 software for rapid proteomics tools development. *Bioinformatics* **24**: 2534–2536
724

Knox K, Wang P, Kriechbaumer V, Tilsner J, Frigerio L, Sparkes I, Hawes C, Oparka KJ (2015) Putting the squeeze on PDs - a role for RETICULONS in primary plasmodesmata formation. *Plant Physiol* pii: pp006682015

Kumar R, Tran LS, Neelakandan AK, Nguyen HT (2012) Higher plant cytochrome b5 polypeptides modulate fatty acid desaturation. *PLoS One* **7**(2):e31370

Lee H, Sparkes I, Gattolin, S, Dzimitrowicz N, Roberts LM, Hawes C, Frigerio L (2013) An Arabidopsis reticulon and the atlastin homologue RHD3-like2 act together in shaping the tubular endoplasmic reticulum. *New Phytol* **197**(2): 481–489

Lerouxel O, Mouille G, Andème-Onzighi C, Bruyant MP, SévenoM, Loutelier-Bourhis C, Driouich A, Höfte H, Lerouge P (2005) Mutants in DEFECTIVE GLYCOSYLATION, an Arabidopsis homolog of an oligosaccharyltransferase complex subunit, show protein underglycosylation and defects in cell differentiation and growth. *Plant J* **42**(4): 455–68

Levy A, Zheng JY, Lazarowitz SG (2015) Synaptotagmin SYTA Forms ER-Plasma Membrane Junctions that Are Recruited to Plasmodesmata for Plant Virus Movement. *Curr Biol* pii: S0960-9822(15)00680–6

Lewis JD, Lazarowitz SG (2010) Arabidopsis synaptotagmin SYTA regulates endocytosis and virus movement protein cell-to-cell transport. *Proc Natl Acad Sci U S A* **9**;107(6): 2491–6

Lin C-C, Seikowski J, Pérez-Lara A, Jahn R, Höbartner C, Jomo Walla PJ (2014) Control of membrane gaps by synaptotagmin-Ca^{2+} measured with a novel membrane distance ruler. *Nature Communications* **5**: 5859

Marín M, Thallmair V, Ott T (2012) The intrinsically disordered N-terminal region of AtREM13 remorin protein mediates protein-protein interactions. *J Biol Chem* **16**;287(47): 39982–91

Maggio C Barbante A, Ferro F, Frigerio L, Pedrazzini E (2007) Intracellular sorting of the tail-anchored protein cytochrome b5 in plants: a comparative study using different isoforms from rabbit and Arabidopsis. *J Exp Bot* **58**(6): 1365–79

762 Maule AJ (2008) Plasmodesmata: structure, function and biogenesis. *Curr Opin Plant Biol* **11**:
763 680–686
764
765 Monaghan J, Zipfel C (2012) Plant pattern recognition receptor complexes at the plasma
766 membrane. *Curr Opin Plant Biol* **15**(4): 349-57
767
768 Mongrand S, Stanislas T, Bayer EM, Lherminier J, Simon-Plas F (2010) Membrane rafts in
769 plant cells. *Trends Plant Sci* 15(12): 656–63
770
771 Nagano M, Ihara-Ohori Y, Imai H, Inada N, Fujimoto M, Tsutsumi N, Uchimiya H, Kawai-
772 Yamada M (2009) Functional association of cell death suppressor, Arabidopsis Bax inhibitor-
773 1, with fatty acid 2-hydroxylation through cytochrome b_5. *Plant J* **58**: 122–134
774
775 Naulin PA, Alveal NA, Barrera NP (2014) Toward atomic force microscopy and mass
776 spectrometry to visualize and identify lipid rafts in plasmodesmata. *Front Plant Sci* **30**(5): 234
777
778 Nelson DC, Flematti GR, Riseborough JA, Ghisalberti EL, Dixon KW, Smith SM
779 (2010) Karrikins enhance light responses during germination and seedling development
780 in Arabidopsis thaliana. *Proc Natl Acad Sci U S A* **13**;107(15): 7095–100
781
782 Nesvizhskii AI, Keller A, Kolker E, Aebersold R (2003) A statistical model for identifying
783 proteins by tandem mass spectrometry. *Anal Chem* **75**(17): 4646–4658
784
785 Oparka KJ, Prior DA, Santa Cruz S, Padgett HS, Beachy RN (1997) Gating of
786 epidermal plasmodesmata is restricted to the leading edge of expanding infection sites of
787 tobacco mosaic virus (TMV). *Plant J* **12**(4): 781–9
788
789 Osterrieder A Carvalho CM, Latijnhouwers M, Johansen JN, Stubbs C, Botchway S, Hawes C
790 (2009) Fluorescence lifetime imaging of interactions between Golgi tethering factors and small
791 GTPases in plants. *Traffic* **10**(8): 1034–46
792
793 Overall RL, Blackman LM (1996) A model of the macro-molecular structure of
794 plasmodesmata. *Trends Plant Sci* **1**: 307–311
795
796 Palade G (1975) Intracellular aspects of the process of protein synthesis. *Science* **189**: 347–
797 58
798

Pattison RJ, Amtmann A (2009) N-glycan production in the endoplasmic reticulum of plants. *Trends Plant Sci* **14**(2): 92–9

Pérez-Sancho J, Vanneste S, Lee E, McFarlane HE, Esteban Del Valle A, Valpuesta V, Friml J, Botella MA, Rosado A (2015) The Arabidopsis synaptotagmin1 is enriched in endoplasmic reticulum-plasma membrane contact sites and confers cellular resistance to mechanical stresses. *Plant Physiol* **168**(1), 132–43

Perraki A, Cacas JL, Crowet J M, Lins L, Castroviejo M, German-Retana S, Mongrand S, Raffaele S (2012) Plasma membrane localization of StREM13 remorin is mediated by conformational changes in a novel C-terminal anchor and required for the restriction of PVX movement. *Plant Physiol* **160**: 624–637

Perraki A, Binaghi M, Mecchia MA, Gronnier J, German-Retana S, Mongrand S, Bayer E, Zelada AM, Germain V (2014) StRemorin13 hampers Potato virus X TGBp1 ability to increase plasmodesmata permeability, but does not interfere with its silencing suppressor activity. *FEBS Lett* **2**;588(9): 1699–705

Raffaele S, Bayer E, Lafarge D, Cluzet S, German Retana S, Boubekeur T, Leborgne-Castel N, Carde JP, Lherminier J, Noirot E, Satiat-Jeunemaître B, Laroche-Traineau J, Moreau P, Ott T, Maule AJ, Reymond P, Simon-Plas F, Farmer EE, Bessoule JJ, Mongrand S (2009) Remorin, a solanaceae protein resident in membrane rafts and plasmodesmata, impairs potato virus X movement. *Plant Cell* **21**(5): 1541–55

Schapire AL, Voigt B, Jasik J, Rosado A, Lopez-Cobollo R, Menzel D, Salinas J, Mancuso S, Valpuesta V, Baluska F, Botella MA (2008) Arabidopsis synaptotagmin 1 is required for the maintenance of plasma membrane integrity and cell viability. *Plant Cell* **20**(12): 3374–88

Schoberer J, Botchway SW (2014) Investigating protein-protein interactions in the plant endomembrane system using multiphoton-induced FRET-FLIM. *Methods Mol Biol* **1209**: 81–95

Scholl RL, May ST, Ware DH (2000) Seed and molecular resources for Arabidopsis. *Plant Physiol* **124**(4): 1477–80

Sparkes I, Runions J, Hawes C, Griffing L (2009) Movement and remodeling of the endoplasmic reticulum in nondividing cells of tobacco leaves. *Plant Cell* **21**: 3937–3949

836
837 Sparkes IA, Tolley N, Aller I, Svozil J, Osterrieder, A, Botchway S, Mueller C, Frigerio L,
838 Hawes C (2010) Five arabidopsis reticulon isoforms share endoplasmic reticulum location,
839 topology, and membrane-shaping properties. *Plant Cell* **22**: 1333–1343
840
841 Stubbs CD, Botchway SW, Slate SJ, Parker AW (2005) The use of time-resolved fluorescence
842 imaging in the study of protein kinase C localisation in cells. *BMC Cell Biol* **26**: 22
843
844 Tapken W, Murphy AS (2015) Membrane nanodomains in plants: capturing form, function,
845 and movement. *J Exp Bot* **66**(6): 1573–86
846
847 Tilsner J, Amari K, Torrance L (2011) Plasmodesmata viewed as specialized membrane
848 adhesion sites. *Protoplasma* **248**(1): 39–60
849
850 Tilsner J, Linnik O, Louveaux M, Roberts IM, Chapman SN, Oparka KJ (2013) Replication and
851 trafficking of a plant virus are coupled at the entrances of plasmodesmata. *J Cell Biol* 201(7):
852 981–995
853
854 Tolley N, Sparkes IA, Hunter PR, Craddock CP, Nuttall J, Roberts LM, Hawes C, Pedrazzini
855 E, Frigerio L (2008) Overexpression of a plant reticulon remodels the lumen of the cortical
856 endoplasmic reticulum but does not perturb protein transport. *Traffic* **8**: 94–102
857
858 Tolley N, Sparkes I, Craddock CP, Eastmond PJ, Runions, J, Hawes C, Frigerio L (2010)
859 Transmembrane domain length is responsible for the ability of a plant reticulon to shape
860 endoplasmic reticulum tubules in vivo. *Plant J* **64**(3): 411–418
861
862 Tucker EB, Boss WF (1996) Mastoparan-Induced Intracellular Ca2+ Fluxes May Regulate
863 Cell-to-Cell Communication in Plants. *Plant Physiol* **111**(2): 459–467
864
865 Uchiyama A, Shimada-Beltran H, Levy A, Zheng JY, Javia PA, Lazarowitz SG (2014) The
866 Arabidopsis synaptotagmin SYTA regulates the cell-to-cell movement of diverse plant viruses.
867 *Front Plant Sci* **6**: 584
868
869 Vitale A, Denecke J(1999) The endoplasmic reticulum – gateway of the secretory
870 pathway. *The Plant Cell* 11: 615–*628*
871

872 Wang P, Hawkins TJ, Richardson C Cummins I, Deeks MJ, Sparkes I, Hawes C, Hussey PJ
873 (2014) The plant cytoskeleton, NET3C, and VAP27 mediate the link between the plasma
874 membrane and endoplasmic reticulum. *Curr Biol* **16**;24(12): 1397-405
875
876 Winter D, Vinegar B, Nahal H, Ammar R, Wilson GV, Provart NJ (2007) An "Electronic
877 Fluorescent Pictograph" browser for exploring and analyzing large-scale biological data
878 sets. *PLoS One* **8**;2(8):e718
879
880 Xu XM, Wang J, Xuan Z, Goldshmidt A, Borrill PG, Hariharan N, Kim JY, Jackson D
881 (2011) Chaperonins facilitate KNOTTED1 cell-to-cell trafficking and stem cell function.
882 *Science* **26**;333(6046): 1141–4
883
884 Yamazaki T, Takata N, Uemura M, Kawamura Y (2010) Arabidopsis synaptotagmin SYT1, a
885 type I signal-anchor protein, requires tandem C2 domains for delivery to the plasma
886 membrane. *J Biol Chem* **23**;285(30): 23165–76
887
888 Zauber H, Burgos A, Garapati P, Schulze WX (2014) Plasma membrane lipid-
889 protein interactions affect signaling processes in sterol-biosynthesis mutants
890 in Arabidopsis thaliana. *Front Plant Sci* **18**;5: 78